Computational analysis of coned-face spiral groove gas seals using the finite element method

Marco Tulio C. Faria

Departamento de Engenharia Mecanica
Universidade Federal de Minas Gerais
Av. Antonio Carlos, 6627 - Belo Horizonte
MG – 31270-901 – Brasil
mtfaria@demec.ufmg.br

ABSTRACT. *In this work, an efficient finite element procedure for high speed thin gas film lubrication problems, which is based on the Galerkin weighted residual method with high order shape functions, is employed to analyze the effects of the face coning on spiral groove face seal performance. Opening force, dynamic force coefficients and leakage flow are determined for different face seal coning angles and operating conditions. Finite element predictions bring some insights into the influence of the face coning on gas-lubricated spiral groove face seal performance characteristics at high speeds.*

RÉSUMÉ. *Dans ce travail, un efficace procédé numérique pour des problèmes de film de lubrification à gaz de haute vitesse, basé sur la méthode des éléments finis des résidus ponderés de Galerkin avec fonction de forme d'ordre élevé, est employé pour l'analyse des effets de la face conique sur l'efficacité d'une garniture en spirale. Les coefficients des forces dynamique et d'ouverture et le débit de fuite de gaz sont déterminés pour différents angles de la face conique et différentes conditions d'opération. Les previsions obtenues avec l'analyse numérique apportent quelque connaissance de l'influence de la conicité de la face par rapport aux caractéristiques d'efficacité de la garniture pour des vitesses élevées du gaz.*

KEYWORDS: *face seals, grooved seals, spiral grooves, coning effects, gas lubrication.*

MOTS-CLÉS : *garniture, garniture frisée, garniture en spirale, effets de conicité, lubrification à gaz.*

REEF – 14/2005. Finite elements in tribology, pages 181 to 194

1. Introduction

Gas bearings and noncontacting gas seals are finding increase use in machinery applications that require low energy consumption and an oil-free environment. The development of efficient sealing systems for rotating machinery in processing industries has been demanded by strict environmental protection laws, which require the virtual elimination of release of harmful work fluids into the atmosphere. Advances in the fluid sealing technology have been accompanied by the development of efficient and accurate numerical methods capable of predicting the seal behavior under stringent operating conditions.

The spiral groove is one of the most successful groove geometries used in gas face seals. Efficient unidirectional spiral groove gas face seals (SGGFSs) have been widely employed in industrial machinery (Burgmann, 1997). Spiral grooves are introduced into face seal designs mainly to increase their load capacity and decrease fluid leakage (Muijdermann, 1966). Even though gas face seals have been largely used in high speed rotating machinery, predictions and experimental measurements of SGGFS static and dynamic performance characteristics at high speeds have not been reported in the literature. At high operating speeds, coning on the face seal due to high pressures and thermal effects can strongly affect the seal performance.

The finite element method (FEM) has been largely used in thin gas film lubrication problems due to its ability to represent complex seal geometries and associated boundary conditions. The Reynolds equation for compressible fluids is a convective-diffusion transport equation. At high speeds, the advection transport terms dominate the gas flow. Reddi and Chu (1970) pioneered the application of the FEM to gas lubricated spiral groove face seals using an incremental formulation. Procedures based either on central finite difference schemes or on the classical Galerkin weighted residual method usually exhibit numerical oscillations in the solution of high speed thin gas film flows, where convective flow terms are important. Upwind schemes have been used to build efficient FEM procedures able to render numerically stable solutions for the Reynolds equation at high speeds. FEM upwind schemes in gas lubrication are generally based on the Petrov-Galerkin weighted residual method and can be implemented either using non-symmetrical weighting functions (Heinrich *et al.*, 1977) or special numerical integration schemes of the advection terms (Hughes, 1978). Bonneau *et al.* (1993) developed one of the few upwind FEM schemes for spirally grooved gas face seals, however they presented the seal performance characteristics only at low speeds. Upwind FEM schemes not only require special numerical integration procedures for the advection terms of the Reynolds equation but also introduce numerical artificial diffusion into the solution.

A finite element study of gas-lubricated spiral groove face seals (SGGFSs) is performed by using a novel finite element procedure specially devised for high-speed thin gas film lubrication problems. This procedure is based on the Galerkin weighted residual method with high order shape functions, which are derived from an approximated solution to the non-linear Reynolds equation within an element

(Faria, 2001). The high-order FEM scheme has been successfully implemented to predict the seal face misalignment effects on SGGFSs operating at high speeds (Faria, 2004) disregarding the face coning effects. The high-order shape functions not only eliminate the need of special integration schemes for the convective terms but also do not introduce artificial diffusion into the solution (Faria, 1999). The main concern of this work is to analyze the effects of the face coning on the static performance characteristics of gas SGGFSs operating at high speeds. At high speeds, the viscous energy dissipation and large pressure ratios may introduce coning on the seal faces. Seal opening force, flow leakage rate and dynamic force coefficients are predicted for coned gas SGGFSs at high speeds.

2. Gas SGGFS model

Figure 1 shows the geometry and parameters of a SGGFS. The seal configurations are described following the same procedure as that used by Faria (2001). The seal geometry includes the ridge clearance c, the groove depth c_g, the ridge width w_r, the groove width w_g, the number of grooves N_g, the groove angle β, the seal inner radius r_i, the seal outer radius r_o, the seal grooved portion inner radius r_{gi} and the seal grooved portion outer radius r_{go}. The groove depth ratio $\delta = c_g / c$ and groove width ratio $\alpha_g = w_g / (w_r + w_g)$ are dimensionless geometric parameters.

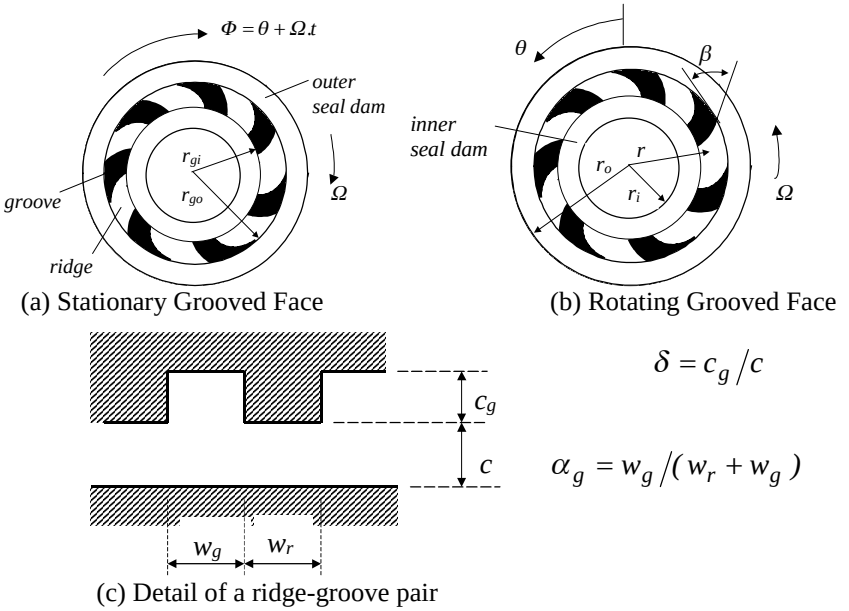

(a) Stationary Grooved Face (b) Rotating Grooved Face

(c) Detail of a ridge-groove pair

$$\delta = c_g / c$$

$$\alpha_g = w_g / (w_r + w_g)$$

Figure 1. *Geometry and physical parameters of a SGFS with rotating and stationary grooved surfaces*

The seal configuration is described in relation to a coordinate system attached to the grooved seal face. The (r,θ, z) coordinate system is attached to the rotating grooves at speed Ω (Figure 1b). The (r,Φ, z) coordinate system is attached to the stationary face (Figure 1a). The relation between the two coordinate systems is given by $\Phi = \theta + \Omega.t$.

The laminar flow of an isothermal, isoviscous ideal gas within the film lands of a spirally grooved face seal is described by (Faria,2001)

$$\frac{1}{r}\frac{\partial}{\partial\theta}\left(\frac{ph^3}{12\mu}\frac{1}{r}\frac{\partial p}{\partial\theta}\right)+\frac{1}{r}\frac{\partial}{\partial r}\left(\frac{ph^3}{12\mu}r\frac{\partial p}{\partial r}\right)=\frac{B\Omega}{2r}\frac{\partial}{\partial\theta}(rph)+\frac{\partial(ph)}{\partial t} \quad [1]$$

Here, p represents the hydrodynamic pressure, h is the fluid film thickness, and μ is the fluid viscosity. B is a parameter that describes the groove rotation direction. Table 1 shows the values of B for the different seal configurations (Faria, 2001).

Table 1. *The groove rotation direction parameter with seal configuration*

Groove Angle (β) Range	Stationary Grooves	Rotating Grooves
$0^o < \beta < 90^o$	Outward Pumping (B = -1)	Inward Pumping (B = 1)
$90^o < \beta < 180^o$	Inward Pumping (B = 1)	Outward Pumping (B = -1)

The seal is subjected to pressures p_i and p_o at its inner and outer radii r_i and r_o, respectively. Typically $p_o > p_i$.

$$p(r_i,\theta,t) = p_i \text{ and } p(r_o,\theta,t) = p_o \quad [2]$$

The fluid film thickness is described accounting for the face coning effects. The face coning is caused either by thermal distortions due to viscous friction (Pan and Sternlicht, 1967) or by mechanical distortions due to the radial pressure gradient (Green, 1987). The coning effects are given by $h_c(r) = (r - r_i)\tan\gamma$, where γ represents the coning angle of the seal surface (see Figure 2). The seal face angular misalignment is not taken into account in this work. The seal mating faces are manufactured with compatible materials of different moduli of elasticity and coefficients of thermal expansion (Burgmann, 1997). The face with lower modulus of elasticity and coefficient of thermal expansion is more likely subjected to face coning. The film thickness h_o at an equilibrium position can be written as

$$h_o(r,\theta) = c + h_c(r), \text{ in the ridge region} \quad [3a]$$

$$h_o(r,\theta) = c + c_g + h_c(r), \text{ in the groove region} \quad [3b]$$

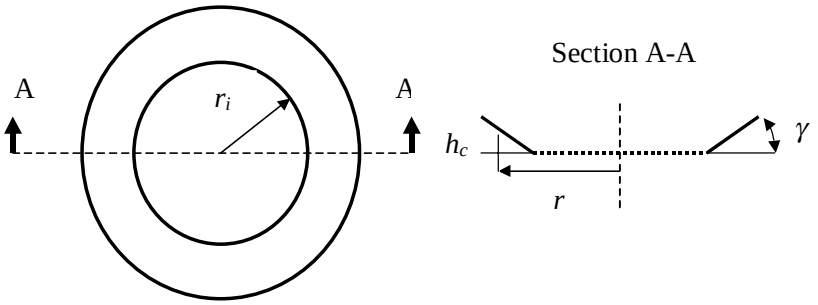

Figure 2. *Schematic view of a coned face mechanical seal*

3. Perturbation analysis

Small dynamic axial (*ΔZ)* perturbations at excitation frequency ω about an equilibrium position of the moving rotating face cause perturbations in the film thickness and pressure distributions. The perturbed film thickness *h(r,θ, t)* and pressure field are given by

$$h(r,\theta,t) = h_o(r,\theta) + \Delta Z.e^{i\omega t};\ i = \sqrt{-1} \qquad [4]$$

$$p(r,\theta,t) = p_o(r,\theta) + p_z(r,\theta)\Delta Z e^{i\omega t} \qquad [5]$$

where p_o represents the zeroth-order pressure field, and p_z is the first-order pressure distribution caused by the small axial perturbations. Expressions for the zeroth- and first-order lubrication equations are obtained by substituting equations [4] and [5] into equation [1]. The zeroth- and first-order equations have the following forms.

$$\frac{1}{r}\frac{\partial}{\partial\theta}\left(\frac{p_o h_o^3}{12\mu}\frac{1}{r}\frac{\partial p_o}{\partial\theta} - \frac{B\Omega r}{2}p_o h_o\right) + \frac{1}{r}\frac{\partial}{\partial r}\left(\frac{p_o h_o^3}{12\mu} r\frac{\partial p_o}{\partial r}\right) = 0 \qquad [6]$$

$$\begin{aligned}&\frac{1}{r}\frac{\partial}{\partial\theta}\left(\frac{3h_o^2}{12\mu r}p_o\frac{\partial p_o}{\partial\theta} + \frac{h_o^3}{12\mu r}\frac{\partial(p_o p_z)}{\partial\theta} - \frac{B\Omega r}{2}(p_z h_o + p_o)\right) + \\ &\frac{1}{r}\frac{\partial}{\partial r}\left[r\left(\frac{3h_o^2}{12\mu}p_o\frac{\partial p_o}{\partial r} + \frac{h_o^3}{12\mu}\frac{\partial(p_o p_z)}{\partial r}\right)\right] = i\omega(p_z h_o + p_o)\end{aligned} \qquad [7]$$

The seal opening force, F_z, and dynamic axial force coefficients, K_{zz} and C_{zz}, are computed by

$$F_z = \iint_{\Pi} (p_o - p_{ref}).r.d\theta.dr \qquad [8]$$

$$K_{zz} + i\omega C_{zz} = -\iint_{\Pi} h.p_z.r.d\theta.dr \qquad [9]$$

where p_{ref} is the reference pressure and Π represents the flow domain within the seal.

4. Finite element modeling

Four-node quadrilateral isoparametric elements are used to represent the flow domain. The finite element procedure is based on the Galerkin weighted residual method. Both zeroth- and first-order pressure fields are interpolated by using the novel class of shape functions, which are derived from an approximate solution to the non-linear Reynolds equation within an element. To show the derivation of the high-order shape functions, the steady-state Reynolds equation for an element (e) is written in relation to an arbitrary system of coordinates (x,y).

$$\frac{\partial}{\partial x}\left(\frac{p_e h_e^{\,3}}{12\mu}\frac{\partial p_e}{\partial x}\right) + \frac{\partial}{\partial y}\left(\frac{p_e h_e^{\,3}}{12\mu}\frac{\partial p_e}{\partial y}\right) = \frac{u}{2}\frac{\partial}{\partial x}(p_e h_e) \qquad [10]$$

For an element (e), $\left(\frac{p_e h_e^3}{12\mu}\right)_1$ and $u.h_e$ are computed for meaningful averaged values. Hence, Equation [10] becomes

$$\frac{\partial^2 p_e}{\partial x^2} + \frac{\partial^2 p_e}{\partial y^2} = \nu\frac{\partial p_e}{\partial x} \quad ; \quad \nu = \frac{6\mu u}{p_e h_e^2} \qquad [11]$$

Equation [11] is a linear partial differential equation, which is solved by separation of variables. For simplicity, the two ordinary differential equations are solved assuming that the constant generated by the separation principle is zero (Faria, 2001). The linearized solution of equation [10] gives the form of the shape functions for the two-dimensional high order Galerkin FEM formulation. These shape functions are expressed in natural coordinates (ξ,η) as

$$\psi_1^e = \frac{1}{2}(1-\eta)\left(\frac{e^{\lambda_e} - e^{\lambda_e\xi}}{e^{\lambda_e} - e^{-\lambda_e}}\right) \quad \psi_2^e = \frac{1}{2}(1-\eta)\left(\frac{e^{\lambda_e\xi} - e^{-\lambda_e}}{e^{\lambda_e} - e^{-\lambda_e}}\right)$$
$$\psi_3^e = \frac{1}{2}(1+\eta)\left(\frac{e^{\lambda_e\xi} - e^{-\lambda_e}}{e^{\lambda_e} - e^{-\lambda_e}}\right) \quad \psi_4^e = \frac{1}{2}(1+\eta)\left(\frac{e^{\lambda_e} - e^{\lambda_e\xi}}{e^{\lambda_e} - e^{-\lambda_e}}\right) \qquad [12]$$

where $\lambda_e = \dfrac{6\mu u L_e}{p_e h_e^2}$ is a local speed or Peclet number. L_e is the averaged element length computed in the circumferential direction. The high-order Galerkin scheme not only eliminates the need of special integration procedures for the advection terms but also does not introduce artificial diffusion into the solution. Then, the finite element zeroth- and first-order lubrication equations are obtained in the following form.

$$K^e_{ji}.p^e_{oi} = q^e_j \text{ , } i,j=1,2,3,4 \qquad [13]$$

$$K^e_{z\,ji}.p^e_{zi} = q^e_{z\,j} + f^e_{z\,j} \text{ , } i,j=1,2,3,4 \qquad [14]$$

where

$$K^e_{ji} = \iint_{\Omega_e} \left\{ \frac{p_o h_o^3}{12\mu} \left(\frac{\partial \psi^e_i}{\partial r}\frac{\partial \psi^e_j}{\partial r} + \frac{1}{r^2}\frac{\partial \psi^e_i}{\partial \theta}\frac{\partial \psi^e_j}{\partial \theta} \right) - \frac{B\Omega h_o}{2}\psi^e_i \frac{\partial \psi^e_j}{\partial \theta} \right\} d\Omega_e \qquad [15]$$

$$q^e_j = -\oint_{\Gamma_e} \psi^e_j \dot{m}_n d\Gamma_e \qquad [16]$$

$$K^e_{z\,ji} = \iint_{\Omega_e} \left[\frac{p^e_o h_o^3}{12\mu} \left(\frac{\partial \psi^e_j}{\partial r}\frac{\partial \psi^e_i}{\partial r} + \frac{1}{r^2}\frac{\partial \psi^e_j}{\partial \theta}\frac{\partial \psi^e_i}{\partial \theta} \right) + \frac{h_o^3}{12\mu} \left(\frac{\partial \psi^e_j}{\partial r}\frac{\partial p^e_o}{\partial r} + \frac{1}{r^2}\frac{\partial \psi^e_j}{\partial \theta}\frac{\partial p^e_o}{\partial \theta} \right) \psi^e_i - \frac{B\Omega h_o}{2}\frac{\partial \psi^e_j}{\partial \theta}\psi^e_i + i\omega h_o \psi^e_j \psi^e_i \right] d\Omega_e \qquad [17]$$

$$q_{z\,j}^{\,e} = -\oint_{\Gamma_e} \psi^e_j \dot{m}_{z\,n} d\Gamma_e \qquad [18]$$

$$f^e_{z\,j} = \iint_{\Omega_e} \left(\frac{-3h_o^2}{12\mu} p^e_o \left(\frac{\partial \psi^e_j}{\partial r}\frac{\partial p^e_o}{\partial r} + \frac{1}{r^2}\frac{\partial \psi^e_j}{\partial \theta}\frac{\partial p^e_o}{\partial \theta} \right) + \frac{B\Omega p^e_o}{2}\frac{\partial \psi^e_j}{\partial \theta} - i\omega p^e_o \psi^e_j \right) d\Omega_e \qquad [19]$$

$\dot{m}_n$ and $\dot{m}_{z_n}$ are the zeroth-order and first-order mass flow rates, respectively, normal to the element boundary The element domain is represented by Ω_e and its boundary by Γ_e. The successive approximations method is employed to solve the

global zeroth-order lubrication obtained by the superposition of element equations [13]. Then, the global first-order lubrication equation is solved using the pre-determined zeroth-order pressure field.

5. Numerical results

A preliminary evaluation of the high-order Galerkin FEM scheme computational efficiency is carried out for an example of high-speed SGGFS with very arcuate and deep grooves, whose parameters are shown on Table 2. The normalized hydrodynamic pressure field (p/p_i) is predicted for a ridge-groove pair using both the high-order and the classical Galerkin FEM schemes. Figure 3.a depicts the the normalized hydrodynamic pressure distribution over a groove-ridge pair obtained by the high-order FEM scheme for 110 elements, while Figure 3.b shows the same distribution computed by the classical Galerkin FEM scheme for 600 elements. The classical Galerkin FEM scheme renders solution numerically unstable at the region of large pressure gradients, *i.e.*, at the trailing edge of the ridge. The normalized pressure field predicted by the classical Galerkin scheme tends very slowly to the solution computed by the high-order scheme as the mesh is refined.

Table 2. *Gas SGFS data for evaluation of computational efficiency*

r_i = 0.00635 m	(*stationary grooves*)	c = 2.75 μm
r_o = 0.01651 m	Λ=1759	c_g = 16.5 μm
β =110^o	ρ =1.12 kg/m^3	μ = 32.37x10^{-6} Pa.s
N_g = 12 grooves		p_i = 0.1 MPa
α_g = 0.8		p_o = 0.1 MPa

Figure 4 depicts comparative results for seal opening force (F_z) versus ridge clearance (c) in a gas SGGFS, whose parameters are given in Table 3. Xue and Stolarski employed an upwind control volume method to analyze SGGFSs operating at low and medium operating speeds. The high-order FEM scheme (squares) produces results practically identical to those obtained by Xue and Stolarski (circles). Also, the validation of leakage flow rate computation was performed for narrow flat mechanical face seals. The predictions of flow leakage, obtained by the high-order FEM scheme, for gas narrow flat face seals, agree very well with the results generated by the approximated analytical solution. Flow leakage rate comparisons are omitted here for brevity.

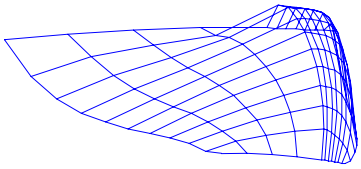

(a) Solution by the high-order Galerkin FEM with 110 elements

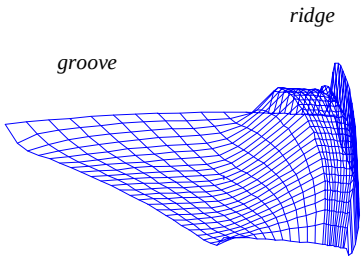

(b) Solution by the classical Galerkin FEM with 600 elements

Figure 3. *Normalized pressure field on a ridge-groove pair of a SGGFS computed by the high-order and classical FEM schemes (Λ=1759)*

Table 3. *SGFS parameters for validation*

r_i = 0.062 m	(*stationary grooves*)	*c* varies
r_{gi} = 0.069 m	Ω = *4774.7 rpm*	c_g = 6 μm
r_o = 0.0805 m	ρ =1.09 kg/m^3	μ = 18x10^{-6} Pa.s
β = 161.4^o		p_i = 0.1 MPa
N_g = 12 grooves	*352 elements for each ridge-groove pair (22 circumferential and 16 radial elements)*	p_o = 0.3 MPa
α_g = 0.567		Λ *varies from 13.7 to 218.7*

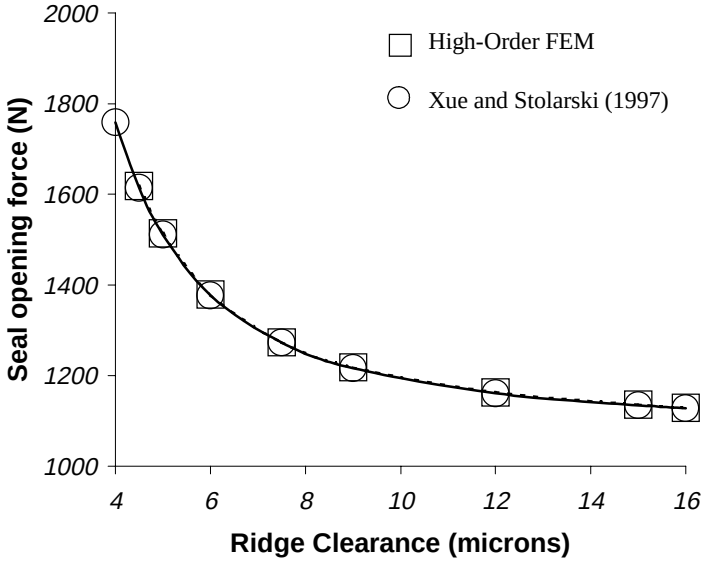

Figure 4. *Comparative results for seal opening force*

Table 4. *Gas SGGFS baseline parameters*

	Stationary grooves	
r_i = 0.07112 m	$\beta = 160^o$	p_i = 0.101 MPa
r_{gi} = 0.076454 m	α_g = 0.5	p_o = 0.505 MPa
r_o = 0.0889 m	N_g =12	Λ = 300 or 1,253
$c = c_g$ = 2.54 μm	$\mu = 10.963 \times 10^{-6}$ Pa.s	(Ω = 3,600 or 15,000 rpm)
	Mesh: 1,320 elements	
	(132 circumferential x 10 radial elements)	

The performance of a perfectly symmetric, aligned SGGFS operating at high speeds is evaluated for positive ($\gamma > 0$) and negative ($\gamma < 0$) coning angles. Rubbing contact between the seal mating faces occurs at approximately $\gamma = -0.008^o$. In this study, the minimum value of coning parameter corresponds to an almost zero outer clearance (about 90% of reduction), while the maximum coning parameter corresponds to an outer clearance four times larger than the seal inner clearance. The seal clearance at the outer radius increases for $\gamma > 0$ and decreases for $\gamma < 0$. Table 4 provides the seal baseline parameters. Figure 5 shows the variation of the

dimensionless flow rate ($\overline{Q}$) and seal opening force ($\overline{F}_z$) versus the dimensionless coning parameter computed at two values of speed number, $\Lambda = 6\mu\Omega r_o^2 / (p_{ref} c^2)$. By using different scales for negative and positive coning angles for graphical representation purpose, dimensionless coning parameter ($\overline{\gamma}$) is defined as

$$\overline{\gamma} = \gamma . (\pi . r_o / 180 . c) \quad \text{for positive } \gamma \qquad [20]$$

$$\overline{\gamma} = 5\gamma . (\pi . r_o / 180 . c) \quad \text{for negative } \gamma \qquad [21]$$

As the outer clearance decreases (γ decreases), the flow resistance increases resulting in higher opening force and lower inward flow. $\overline{Q}$ and $\overline{F}_z$ increase as the speed number (Λ) increases due to the increase in the hydrodynamic pressure over the seal domain.

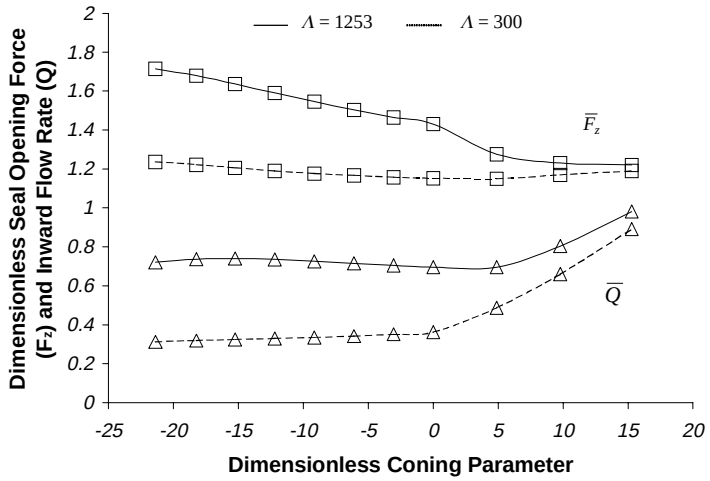

Figure 5. *Dimensionless seal opening force and inward flow rate versus the dimensionless coning angle at two speed numbers, Λ=300 (dotted line) and Λ=1253 (solid line)*

Figure 6 shows the static axial stiffness coefficients versus the coning parameter at moderate (dotted line) and high speed numbers (solid line). These coefficients are evaluated at a very low axial excitation frequency (σ = 1). For large γ (γ > 0.045 degrees) the stiffness coefficients tend to very low asymptotic values. Coned faces with increasing radial clearance (divergent coning) have low stiffness to axial motions. On the other hand, small convergent coning angles (negative γ) can enhance the seal performance characteristics.

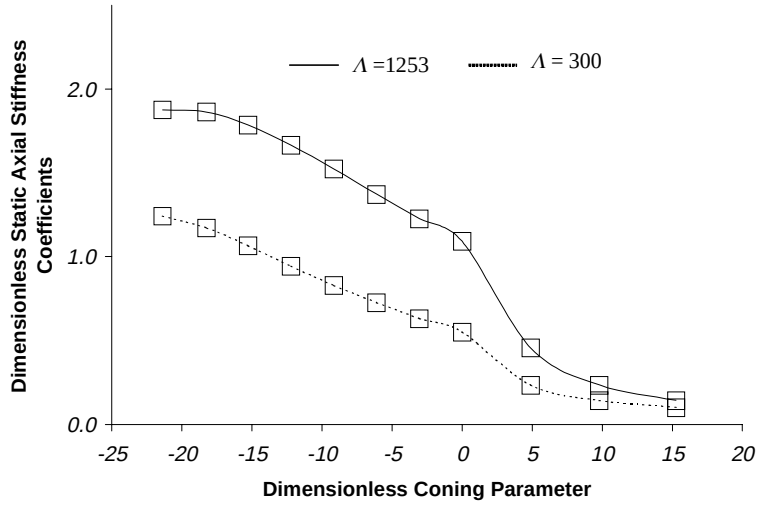

Figure 6. *Dimensionless seal static axial stiffness coefficients versus the dimensionless coning angle at two speed numbers, Λ =300 (dotted line) and Λ =1253 (solid line)*

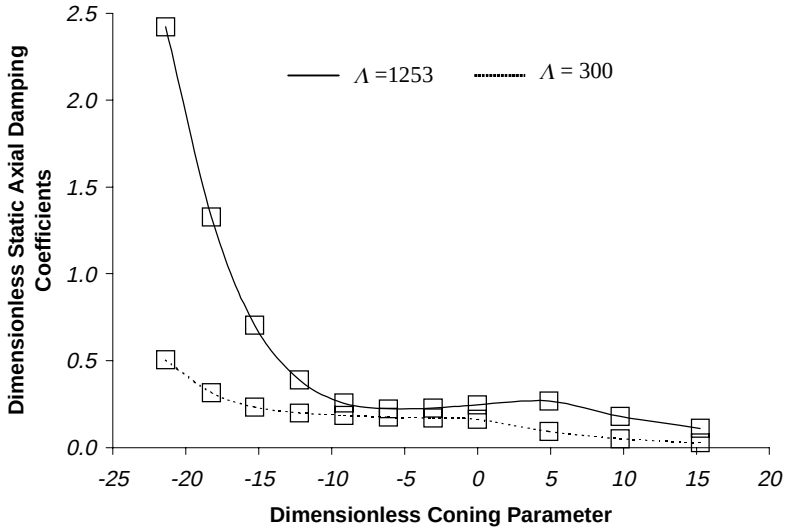

Figure 7. *Dimensionless seal static axial damping coefficients versus the dimensionless coning angle at two speed numbers, Λ =300 (dotted line) and Λ =1253 (solid line)*

The variation of the dimensionless static axial damping coefficients in relation to the coning parameter is shown in Figure 7. Stiffness and damping increase as the outer clearance decreases ($\bar{\gamma} < 0$) because of the increasing flow resistance. For small outer clearances ($\bar{\gamma} < -12$), the direct axial damping ($\overline{C}_{zz}$) increases significantly as the coning angle decreases at high speed number ($\Lambda = 1253$).

Solid lines represent the characteristics evaluated at Λ=1 253 and dotted lines represent those at Λ=300. The dimensionless variables used in the analysis of the coning effects are computed as $\overline{F}_z = F_z \big/ p_{av}.\pi.(r_o^2 - r_i^2)$; $\overline{K}_{zz} = K_{zz}.c \big/ (p_{av}.\pi.(r_o^2 - r_i^2))$; $\overline{C}_{zz} = C_{zz}.c.\Omega \big/ (p_{av}.\pi.(r_o^2 - r_i^2))$; and $\overline{Q} = \pi.p_{av}(c + c_g)^3(p_i - p_o) \big/ (6.\mu.\ln(r_o / r_i))$; where $p_{av} = (p_o + p_i)/2$.

6. Conclusion

A finite element study of the influence of the face coning on the behavior of gas-lubricated spiral groove face seals operating at high speeds is carried out by using an efficient procedure specially devised for thin gas film lubrication problems. It is clearly shown that the coning effects have a strong influence on the gas seal performance mainly at negative coning angles due to the increasing flow resistance associated with the reduction of the outer clearance.

7. References

Bonneau D., Huitric J., Tournerie B., "Finite Element Analysis of Grooved Gas Thrust Bearings and Grooved Gas Face Seals", *ASME Journal of Tribology*, Vol. 115, 1993, pp. 348-354.

Burgmann Dichtungswerke GmbH & Co., *Gas Lubricated Mechanical Face Seals*, Wolfratshausen, Germany, 1997.

Faria M.T.C., "A Novel Finite Element Procedure for Hydrodynamic Thin Gas Film Lubrication", *Proceedings of the XV Brazilian Congress of Mechanical Engineering*, Águas de Lindóia, São Paulo, November 22-26, 1999, pp. 1-10.

Faria M.T.C., "An Efficient Finite Element Procedure for Analysis of High-Speed Spiral Groove Gas Face Seals", *ASME Journal of Tribology*, Vol. 123, No. 1, 2001, pp. 205-210.

Faria M.T.C., "Finite Element Analysis of the Misalignment Effects on the Dynamic Force Coefficients of Spiral Groove Gas Face Seals", *JSME International Journal*, Series C, Vol. 47, No. 1, 2004, pp. 289-296.

Green I., "The Rotor Dynamic Coefficients of Coned-Face Mechanical Seals with Inward and Outward Flow", *ASME Journal of Tribology*, Vol. 109, 1987, pp. 129-135.

Heinrich J.C., Huyakorn P.S., Zienkiewicz O.C., Mitchell A.R., "An Upwind Finite Element Scheme for Two-dimensional Convective Transport Equation", *International Journal for Numerical Methods in Engineering*, Vol. 11, 1977, pp. 131-143.

Hughes T.J.R., "A Simple Scheme for Developing "Upwind" Finite Elements", *International Journal for Numerical Methods in Engineering*, Vol. 12, 1978, pp. 1359-1365.

Muijderman E.A., *Spiral Groove Bearings*, Philips Technical Library, Springer-Verlag, New York, 1966.

Pan C.H.T., Sternlicht B., "Thermal Distortion of Spiral-Grooved Gas Lubricated Thrust Bearing Due to Self-Heating", *ASME Journal of Lubrication Technology*, 1967, pp. 197-202.

Reddi M.M., Chu T.Y., "Finite Element Solution of the Steady-state Compressible Lubrication Problem", *ASME Journal of Lubrication Technology*, 1970, pp. 495-503.

Xue Y., Stolarski T.A., "Numerical Prediction of the Performance of Gas-Lubricated Spiral Groove Thrust Bearings", *Proceedings of the Institution of Mechanical Engineers, Part J: Journal of Engineering Tribology*, Vol. 211, 1997, pp. 117-128.